Journal of
Applied Crystallography
ISSN 0021-8898

Received 12 October 2001
Accepted 27 February 2002

A microspectrophotometer for UV–visible absorption and fluorescence studies of protein crystals

Dominique Bourgeois,[a,b]* Xavier Vernede,[b] Virgile Adam,[a,b] Emanuela Fioravanti[a,b] and Thomas Ursby[a,b,c]

[a]ESRF, BP 220, 38043 Grenoble CEDEX, France, [b]LCCP, UMR 9015, IBS, 41 Rue Jules Horowitz, 38027 Grenoble CEDEX 1, France, and [c]MAX-lab, Lund University, POB 118, S-22100 Lund, Sweden. Correspondence e-mail: bourgeoi@lccp.ibs.fr

Absorption microspectrophotometry has been shown to be of considerable help to probe crystalline proteins containing chromophores, metal centres, or coloured substrates/co-factors. Absorption spectra contribute to the proper interpretation of crystallographic structures, especially when transient intermediate states are studied. Here it is shown that fluorescence microspectrophotometry might also be used for such purposes if endogenous fluorophores are present in the macromolecule or when exogenous fluorophores are added and either bind to the protein or reside in the solvent channels. An off-line microspectrophotometer that is able to perform low-temperature absorption and fluorescence spectroscopy on crystals mounted in cryo-loops is described. One-shot steady-state emission spectra of outstanding quality were routinely collected from several samples. In some cases, crystals with optical densities that are too low or too high for absorption studies can still be tackled with fluorescence microspectrophotometry. The technique may be used for simple controls such as checking the presence, absence or redox state of a fluorescent substrate/co-factor. Potential applications in the field of kinetic crystallography are numerous. In addition, the possibility to probe key physico-chemical parameters of the crystal, such as temperature, pH or solvent viscosity, could trigger new studies in protein dynamics.

1. Introduction

Macromolecular X-ray crystallography provides a wealth of three-dimensional structural information that greatly contributes to elucidating protein functions. Considerable insight into the understanding of enzymatic reaction mechanisms can be gained from the knowledge of three-dimensional structures of complexes such as protein–substrate, protein–product, or even protein–transition-state analogs. Based on recent advances in cryo-crystallography (Garman & Schneider, 1997), methods in kinetic crystallography (Schlichting, 2000) are also being developed to trap intermediate states along the reaction pathway. In this way, quite complete pictures of catalysis have been obtained with crystallographic methods in a number of cases (Petsko & Ringe, 2000, and references therein).

Whenever an enzymatic reaction is tackled by crystallography, a preliminary but essential step is to study the catalytic competence of the crystallized enzyme and compare it with results obtained in solution (Mozzarelli & Rossi, 1996; Stoddard & Farber, 1995). For such studies, it is an advantage to be able to follow substrate binding, product release, and accumulation of intermediates within the crystal prior to exposure to X-rays. Analytical methods that have been used include high-pressure liquid chromatography (Schlichting *et al.*, 1989), mass spectroscopy (Cohen & Chait, 2001), video absorption spectroscopy (O'Hara *et al.*, 1995) or absorption microspectrophotometry (Mozzarelli & Rossi, 1996, and references therein).

The latter technique can be applied to metallo-enzymes, photosensitive proteins or whenever co-factors, substrates or products are coloured. Being non-destructive, microspectrophotometry allows the same crystal to be used for X-ray experiments. Spectra can be collected at room temperature, possibly in combination with flow-cell devices, but the highest quality spectra are usually obtained with loop-mounted crystals at cryo-temperatures. The technique can be used in a simple manner to check the presence of a substrate or co-factor, or the redox state of the sample. UV–visible spectroscopy has also proven instrumental in designing protocols for efficient triggering of turnover in the crystal and successful trapping of short-lifetime intermediate states (Royant *et al.*, 2000; Genick *et al.*, 1998; Nurizzo *et al.*, 1999). Although spectroscopic changes do not always accompany structural changes (see for example Ren *et al.*, 2001), spectroscopy often serves to identify the structure of intermediates, especially when crystallographic data with only limited resolution are available. Finally, microspectrophotometry can reveal X-ray radiation damage, *e.g.*

reduction of metal centres or disulfide bridges by X-ray induced photoelectrons (Karlsson *et al.*, 2000).

The interest in microspectrophotometry on macromolecular crystals can be widened to the case of fluorescence. Fluorescence in dilute solution is known to be an extremely sensitive technique. Enzymatic assays routinely use fluorescent probes to follow ligand binding, product release, and possibly associated conformational changes in proteins (Eftink, 1997; for studies of crystallographic interest see, for example, Scheidig *et al.*, 1995). Endogenous fluorescence from aromatic residues is also extensively used, for example in protein folding experiments (Eftink & Shastry, 1997). A few pioneering fluorescence measurements on protein single crystals have been carried out at room temperature. Perozzo *et al.* (1988) have shown that emission fluorescence spectra from green fluorescent protein crystals resemble those recorded in solution. A similar study has been conducted on the Y base of yeast tRNA-Phe (Langlois *et al.*, 1975). Willis *et al.* (1991) have followed the fluorescence decay kinetics of tryptophan residues in myoglobin to probe long-range intra- and intermolecular interactions between tryptophyl residues and the heme. In their study of erabutoxin b crystals, Dahms *et al.* (1995) revealed the presence of multiple conformations of tryptophan residues, although a single conformation had been modelled in the structure.

In a large number of cases, fluorescence measurements can be valuable when characterizing crystallized macromolecules. In a similar way to absorption, fluorescence microspectrophotometry may reveal features of the static sample, aid in measuring the enzymatic activity in the crystalline state and facilitate setting-up protocols to trap intermediate species in the crystal. For example, fluorescence from substrates or cofactors such as NADH, NADPH, FMN, FAD, or pyridoxal phosphate may be used to evaluate the binding affinity of such molecules, their redox state, their consumption/production during turnover in the crystal, or even conformational changes along the reaction pathway. Modified substrates, such as ε-ATP, could also be used to perform similar tasks. Alternatively, freely diffusing exogenous fluorophores, such as fluorescein, can be added to the crystallization medium and advantage can be taken of fluorophore–solvent interactions to probe the physico-chemical state of the latter, *e.g.* its pH or viscosity.

In a collaboration between the European Synchrotron Radiation Facility (ESRF, Grenoble, France) and the Institut de Biologie Structurale (IBS, Grenoble, France), we developed an off-line laboratory which provides the user with several instruments to trigger, control and monitor reactions in protein crystals efficiently. The setup includes a microspectrophotometer that can perform both absorption and fluorescence measurements, possibly in tandem. Microspectrophotometers for absorption (Hadfield & Hajdu, 1993, see also http://www.4dx.se; Chen *et al.*, 1994) and fluorescence (Dahms & Szabo, 1997) studies on protein crystals have already been built. In the latter case, crystal mounting cells did neither allow work at cryo-temperatures nor facilitate re-use of the sample for subsequent X-ray analysis. Our approach allows work with loop-mounted crystals (Teng, 1990) at temperatures between 90 K and room temperature. This drastically reduces problems of stray light and makes the device fully compatible with the requirements of modern cryocrystallography (Garman & Schneider, 1997). Measuring spectra at cryo-temperatures also improves the quality of both absorption and fluorescence spectra owing to a lower number of populated vibrational states and to a generally increased fluorescence yield.

In this paper, we describe our microspectrophotometer and show that steady-state fluorescence emission spectra of excellent quality can be recorded in less that 30 ms on protein crystals of standard size containing endogenous or exogenous fluorophores. We present the cases of *Ectothiorhodospira halophila* photoactive yellow protein (PYP), which contains a covalently bound weakly fluorescent 4-hydroxycinamoic acid chromophore, *Haloarcula marismortui* malate dehydrogenase (MalDH), which was co-crystallized with NADH, and *Mycobacterium tuberculosis* thymidilate kinase (Tmpk), which we soaked in a fluorescein solution used as a pH indicator.

2. Description of the microspectrophotometer

A schematic view of the spectrometer assembly is shown in Fig. 1(*a*), and a picture of the apparatus in Fig. 1(*b*). Samples are usually mounted in nylon cryo-loops (Hampton Research) and kept at cryo- or room (see below) temperature. This eliminates most difficulties associated with scattered light and specular reflections frequently encountered when working with capillaries. A stiff mechanical support holds (i) a simple one-circle goniometer (Nonius, ref. 1511900) mounted on a horizontal axis, (ii) an observation stereo-microscope (Olympus, ref. SZ6045 TR) that allows one to observe the sample from above and centre it, and (iii) a rotating arm that maintains two or optionally three identical confocal mirror objectives focusing/collecting UV/visible light to/from the sample. A numerical camera (Olympus, ref. Camedia C3030) is connected to the observation microscope and allows one to observe the sample on a video monitor or to record high-resolution pictures. Space is reserved to position the nozzle of an Oxford cryo-cooler horizontally, co-axially with the goniometer axis, and optionally to place the nozzle of a regulated humidifying gas stream device on a vertical axis, below the sample. This device maintains adequate humidity around the crystal when working at close to room-temperature. Additional mechanical support is available to focus light directly from lasers or from a UV flashlamp (Rapp Optoelectronic, ref. JML-C1) onto the sample.

The objectives are based on reflecting mirrors (Coherent, ref. 250506) and were originally designed by Hadfield & Hajdu (1993) to avoid spherical aberration at the sample position as well as the necessity of quartz optics to access the UV range (see also Schotte, 2000). They are connected to light sources and to spectrometers by optical fibres. Coupling between the fibres and the objectives was modified from that of Hadfield & Hajdu (1993), by replacing a collimating lens at the origin of significant chromatic aberration by a 3 mm diameter pinhole,

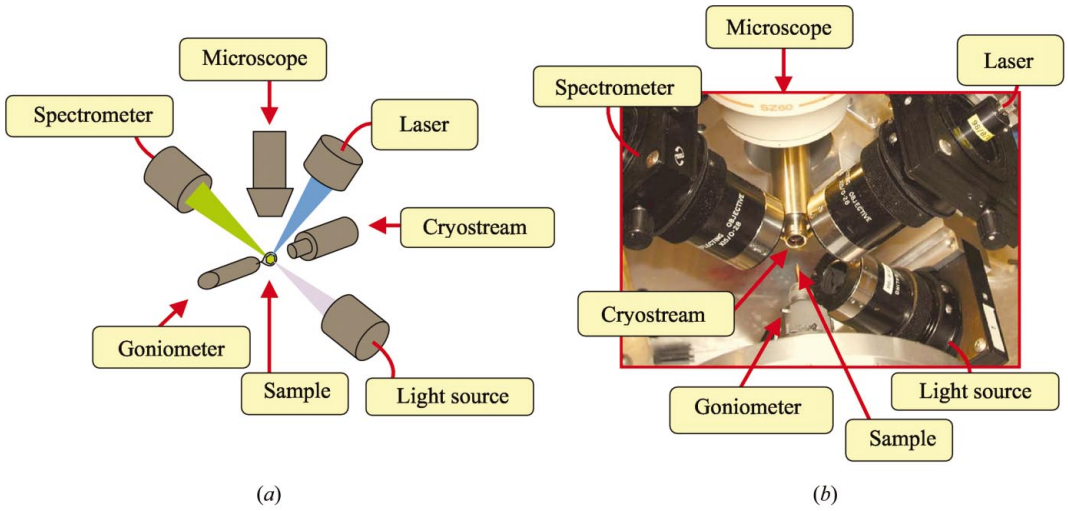

Figure 1
(*a*) Schematic view of the absorption and fluorescence spectrophotometer. (*b*) Corresponding picture of the device.

placed 21 mm away from the fibre tip (U. Genick, personal communication). In this way, a large wavelength bandpass (250–850 nm) can be focused onto a 50 µm diameter spot at the sample position, at the expense of *ca* 40% loss in the transmission efficiency of the objectives. The overall forward transmission efficiency of one objective (power measured at 455 nm through a 100 µm pinhole at the sample position divided by input power) is *ca* 4%. The focus size was measured to be 48 µm [full width at 0.1% (FW0.1%) calculated by fitting a two-dimensional Gaussian to values of measured transmissions through pinholes of diameter 20 µm to 100 µm] with a typical input fibre of 100 µm diameter. In absorption mode, considering residual leaks around the sample dependent on sample size, goniometer sphere of confusion and alignment quality, the instrument response is 99% linear up to an optical density of >2 for a 50 µm diameter sample (respectively >3 for a 100 µm diameter sample). However, the effective linearity range might be lower, depending on sample characteristics, especially due to residual refraction and scattering effects. The crystal orientation has to be optimized in each case and residual leakage results in effective peak broadening. Three light sources are available for absorption measurements: a cw 75 W xenon lamp used in the wavelength range 400–850 nm (Oriel ref. 6263, power supply ref. 68806), a cw 30 W deuterium lamp used in the wavelength range 250–450 nm (Oriel ref. 63163, power supply ref. 68840), and a pulsed 0.325 mJ/1.6 µs xenon lamp (repetition rate 100 Hz) used in the wavelength range 400–850 nm (Oriel ref. 6426, power supply ref. 68825). Light is guided from the light source to the emitting reflecting objective through a narrow optical fibre (Spectraline, ref. FC-UV100-2, typically 100 µm core diameter, NA = 0.22) and from the receiving objective to the spectrometer through a wider optical fibre (Spectraline ref. FC-UV600-2, typically 600 µm core diameter, NA = 0.22). The spectrometer (plug-in PC-2000, Ocean Optics Inc.) consists of a 50 µm entrance slit, a 600 lines mm^{-1} grating and a one-dimensional 2048 pixels CCD chip. It covers the wavelength range 200–850 nm with 2.3 nm resolution. The signal is digitized over 12 bits and the signal to noise ratio exceeds 500 at saturation level. The CCD r.m.s. readout noise amounts to *ca* 1 count, the dark current to 0.07 counts s^{-1} and therefore the dynamic range is about 4000. Two additional 'slave' spectrometer cards are also available and can be used simultaneously with the 'master' spectrometer card described above. One provides enhanced sensitivity in the UV range (200 µm entrance slit, 1800 lines mm^{-1} grating, wavelength range 250–410 nm with 3.3 nm resolution). The other provides enhanced sensitivity over the entire spectral range, at the expense of resolution (200 µm entrance slit, 600 lines mm^{-1} grating, wavelength range 200–850 nm with 8.4 nm resolution). Two cards can be used in tandem if absorption and fluorescence are to be measured alternately.

In fluorescence mode, excitation light is provided with lasers and emission spectra are collected in one-shot. The solid angle covered by the detection objective is *ca* 0.30 steradian. For a hypothetical sample containing 10^{13} fluorophores (case of a crystal of 100 × 50 × 50 µm, with a protein concentration of 7 m*M* and one fluorophore per protein molecule) with a fluorescence quantum yield of 0.1 and optical density 0.1 at 450 nm, theoretical calculations predict that *ca* 20 µW must be available at the sample to produce an emission spectrum filling the spectrometer dynamic range in about 10 ms. Considering the relatively low forward transmission efficiency of the objectives, such a power density cannot be easily achieved with cw light sources coupled to an *e.g.* 1% bandpass monochromator. However, this can easily be achieved with compact lasers. Several lasers are presently or will soon be available to provide excitation light at 266 nm (2 mW) (passively q-switched YAG laser, Nanolase ref. NU-00212–100), 355 nm (4 mW) (passively q-switched YAG laser, Nanolase ref. NV-00212–100), 457 nm (15 mW), 465 nm (14 mW), 472 nm (12 mW), 477 nm (23 mW), 488 nm (60 mW), 496 nm (21 mW), 502 nm (6 mW), and 514 nm (60 mW) (argon ion laser, Melles Griot ref. 35-MAP 321–220), 532 nm (10 mW) (passively q-switched YAG laser, Nanolase ref. NG-01012–

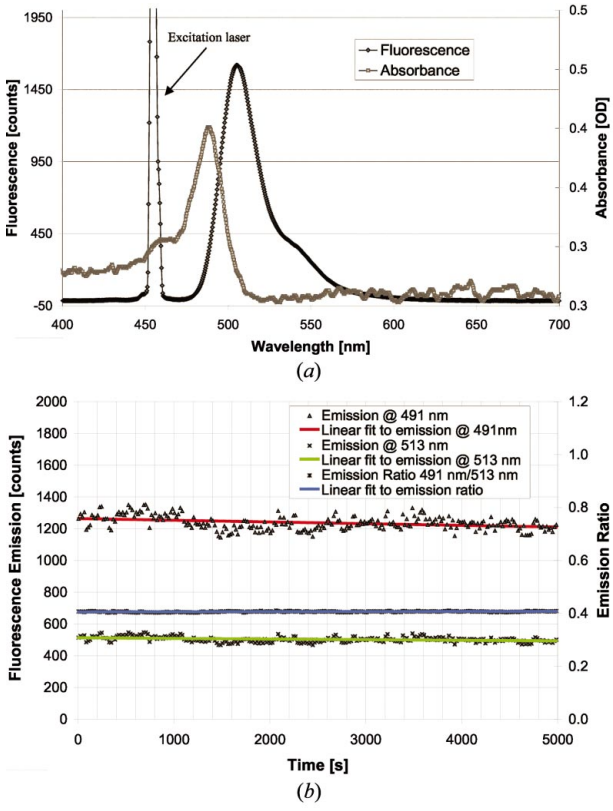

Figure 2
(*a*) Typical absorption and emission fluorescence spectra from a solution of 0.3 m*M* fluorescein in 40% (vol./vol.) glycerol, recorded at 170 K. (*b*) Stability plot recorded over more than one hour with the same sample. The shift in peak wavelength can be best followed by recording the ratio of the intensity at the two inflexion points of the main line (491 and 513 nm). The r.m.s. deviation of this ratio amounts to better than 1%. A shift of the whole spectrum of 0.32 nm (one CCD pixel) would induce a change in this ratio of 6.8%. The achieved stability in peak wavelength is therefore better than 0.1 nm.

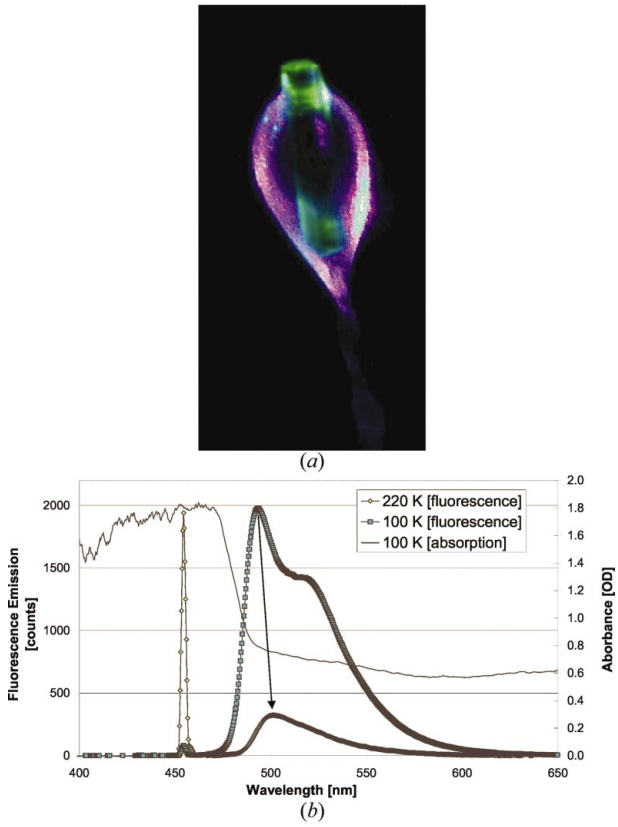

Figure 3
(*a*) A PYP crystal yielding green fluorescence under continuous illumination with blue light. (*b*) Fluorescence emission spectra of a PYP crystal recorded at 100 and 170 K. Superimposed is a (saturated) absorption spectrum collected on the same crystal at 100 K. The arrow highlights the red shift in peak emission wavelength observed as the temperature is raised.

100) and 632.8 nm (20 mW) (helium-neon laser, NEC ref. GLG 5410). To avoid temperature elevation and potential photo-bleaching, fluorescence measurements are generally performed in a pulsed way. Using a mechanical shutter synchronized with the spectrometer CCD readout, spectra with exposure times of typically 10–30 ms are collected at a frequency of 1–10 Hz. To prevent scattered excitation light perturbing the fluorescence spectrum, a long-pass filter is inserted when necessary in front of the detection objective, cutting out light at the excitation wavelength. Depending on sample optical density, which in some cases can be very high (>2), either right-angle or front-face geometry is used (Lakowicz, 1999). The latter geometry allows difficulties associated with strong inner-filtering to be partially overcome at the cost of mostly probing the crystal surface. By using two spectrometer cards in tandem, the two in-line mirror objectives can record fluorescence simultaneously. In this case, if one spectrum is obtained with the right-angle geometry and the other with the front-face geometry, a comparison of both spectra allows an estimation of spectral distortion resulting from inner filtering.

Spectra are analysed on a PC (Windows 98) with the Ocean Optics Inc. Base32 software, which enables kinetic measurements. Raw spectra (see Figs. 2–5) are of excellent quality and do not require correction for the instrument response function, unless absolute spectra are needed. Output files are in ASCII format and can be further processed by any preferred analysis software.

3. Results

Absorption spectra of excellent quality recorded with the described microspectrophotometer have been already published in the literature and will not be discussed here (Nurizzo *et al.*, 1999; Nicolet *et al.*, 2001; Royant *et al.*, 2000, Karlsson *et al.*, 2000).

Fig. 2(*a*) shows a one-shot fluorescence emission spectrum from a 40% (vol./vol.) glycerol solution containing 0.3 m*M* fluorescein. The sample consisted of a *ca* 50 µm thick amorphous film of solution maintained at 170 K in a cryo-loop. The volume probed by the spectrometer amounted to *ca* 0.25 nl. The corresponding absorption spectrum, recorded using a xenon lamp, shows that the optical density of fluorescein amounts to about 0.125 OD. Fluorescence excitation was provided at 455 nm by an argon ion laser. Emission spectra

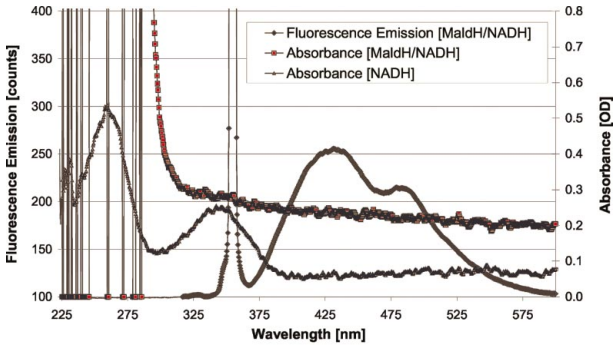

Figure 4
Fluorescence emission spectrum from a MalDH crystal co-crystallized with NADH, recorded at 100 K. The typical fluorescence from reduced NADH is observed, although slightly perturbed by residual scattering from the excitation 355 nm laser. The corresponding absorption spectrum is shown, but does not allow one to detect the presence of reduced NADH. Vertical lines in the wavelength range 225–290 nm result from saturated absorbance. For comparison, an absorption spectrum of a 5 m*M* NADH film solution of *ca* 100 µm thickness shows a clear signal, approximately equivalent to what should be observed in the crystal if reduced NADH had full occupancy.

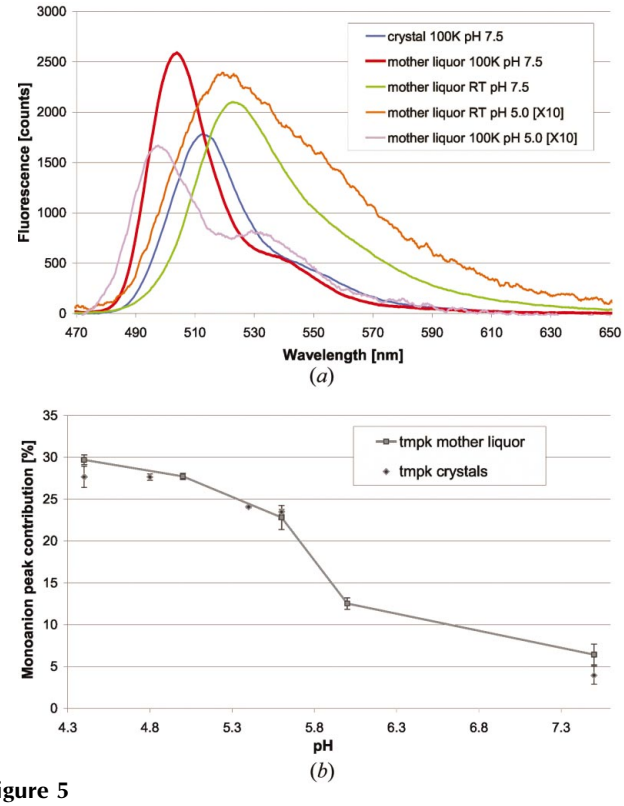

Figure 5
(*a*) Fluorescein emission spectra recorded in various conditions (×10 means scaled up by a factor of 10). Several observations can be made: (i) the fluorescence intensity decreases when the pH is lowered; (ii) the peak wavelength is dependent on pH, but also on temperature and crystalline environment; (iii) the shoulder corresponding to the contribution of the mono-anionic form of fluorescein can be clearly identified at cryo-temperatures, but not at room temperature. (*b*) Relative contribution of the shoulder peak measured as a function of pH at 100 K. pH values are reported as measured at room temperature. Values correspond to the mean of four (respectively three) independent measurements for films of Tmpk mother liquor (respectively for Tmpk crystals). The length of error bars corresponds to twice the r.m.s. deviation from these measurements. Buffers were sodium citrate (pH < 6.0), MES (pH 6.0) and HEPES (pH 7.5). The contribution from the shoulder peak was calculated by subtracting the experimental spectra (with background subtracted and peak surface normalized to 1) to a Gaussian curve initially obtained by fitting the part of a pH 7.5 emission spectrum corresponding to the di-anionic contribution. At each pH, the Gaussian curve was shifted to match the experimental spectrum at the peak wavelength. The obtained difference spectrum was then summed in a fixed wavelength range covering the shoulder peak. At the used concentration of fluorescein, residual inner filtering effects were small. However, these effects, if present, would vary with pH and would imply a slight degradation in the 'contrast' of the titration curve.

were recorded at a frequency of 1 Hz with an exposure time of 20 ms. Although the sample is slightly opaque at this temperature and diffuses light significantly, residual stray radiation from the excitation laser does not interfere with the fluorescence line, which appears of remarkable signal to noise quality. The peak emission, at 505 nm, is significantly blue shifted relative to the value commonly observed at room temperature (*ca* 510 nm). Fig. 2(*b*) shows the stability of the fluorescence emission of the same solution, as recorded by the spectrometer over 5000 s. Counting is reported at two wavelengths of the emission spectrum (491 and 513 nm) located near inflexion points of the latter. A slight linear decay of the fluorescence intensity is observed over time, which is estimated to be *ca* 3% per hour and probably results from photo-bleaching. Instabilities of relatively high frequency (3.3% r.m.s. deviation) are also observed, which result from residual absorption by turbulent wet air circulating around the cold nitrogen stream. The ratio between the two countings, which is a sensitive marker of the peak emission wavelength, is remarkably stable (0.42% r.m.s. deviation).

Fig. 3 shows two one-shot emission spectra from a crystal of PYP, collected at 100 and 220 K. PYP is thought to mediate the build up of a negative phototactic response to blue light (Genick *et al.*, 1998). Rod-shaped crystals of about 50 × 50 × 250 µm were grown in space group $P6_5$. Spectra were obtained in the same conditions as those of Fig. 1. Despite the small size of the crystal, its large optical density in the range 400–470 nm prevented the collection of useful absorption spectra. However, proper orientation of the crystal allowed fluorescence spectra of excellent quality to be obtained, although these mainly probed the sample surface. Similar emission spectra could be obtained using excitation at 355 nm, a wavelength well remote from the absorption maximum of PYP (not shown). This allowed the bulk of the crystal to be probed, but rapidly resulted in serious photo-bleaching of the chromophore. A picture of fluorescent PYP under conditions of continuous illumination at 100 K is shown in Fig. 3(*a*). When the temperature was raised from 100 to 220 K, several features were observed: (i) a 6.2-fold decrease in fluorescence intensity, (ii) a bathochromic shift of the peak emission wavelength from 494 to 502 nm, and (iii) the disappearance of a shoulder at 520 nm.

Fig. 4 shows a fluorescence emission spectrum from a crystal of MalDH in complex with NAD^+/NADH (Dym *et al.*, 1995). MalDH catalyses the NADH-dependent reduction of oxaloacetate to malate. The crystal was kept under aerobic condi-

tions for several months. The oxidation state of the co-factor was therefore in question. The spectrum was obtained at 100 K by averaging ten individual spectra collected in the same conditions as mentioned above, with excitation provided at 355 nm. Since oxidized NAD^+ is non-fluorescent, this spectrum unambiguously revealed the presence of reduced NADH. On the contrary, an absorption spectrum collected on the same crystal showed no peak at *ca* 347 nm, although a spectrum from a fresh 5 m*M* solution of NADH kept in a cryo-loop did show this peak.

Finally, Fig. 5 shows that fluorescein can be used as an efficient pH indicator in frozen protein crystals. On Fig. 5(*a*), it can be seen that at cryo-temperatures, emission spectra from fluorescein display a shoulder on the long-wavelength side of the main peak, which becomes more pronounced as the pH is lowered. This shoulder peak, which is assigned to the mono anionic form of fluorescein, remains non-visible on spectra recorded at room temperature. At cryo-temperatures, computing the relative area of this peak as the pH is varied allows one to obtain 'titration' curves, which are essentially independent of peak intensity and wavelength. Such curves are shown in Fig. 5(*b*), and were derived from spectra recorded at 100 K in amorphous films of the crystallization medium of Tmpk and in crystals of this enzyme, as the pH was varied from 4.4 to 7.5. In both cases, the total fluorescence intensity also decreased significantly when the pH was lowered, but the dependence on variable sample thickness made such measurements less reliable (not shown). It is also interesting to note that at a given pH, the peak emission wavelengths in solution and in crystals were different (Fig. 5*a*). For all samples the concentration of fluorescein was 0.3 m*M*, and the excitation wavelength was 455 nm (close to the isobestic point between the absorption lines of the mono- and di-anionic forms of fluorescein) and the optical density of fluorescein was reproducibly measured at 488 nm to fall in the range 0.1–0.3 OD. Adding fluorescein to the Tmpk crystallization medium did not alter the crystal quality for at least 24 h, as revealed by a high-resolution (1.75 Å) X-ray diffraction data set collected at 100 K on a Tmpk crystal treated in this way. Statistical factors were similar to those obtained without fluorescein, and electron difference density maps did not show any feature that could correspond to putative binding sites for this molecule (not shown). These results are not surprising since the concentration of fluorescein was much lower than that of the enzyme in the crystal (29 m*M*). Therefore, in the absence of any strong affinity of fluorescein for the enzyme, the vast majority of the macromolecules are not perturbed.

4. Discussion and perspectives

The presented results show that our spectrophotometer allows high-quality steady-state fluorescence emission spectra to be readily collected from protein crystals in diverse conditions. Adding the fluorescence option to our absorption micro-spectrophotometer was relatively straightforward, since it required only a modification of the geometry of the setup and the purchase of suitable excitation lasers and synchronization electronics.

Test spectra from fluorescein collected in one shot and in a few milliseconds show high accuracy and reproducibility. We conclude from Fig. 2 that relative changes in fluorescence intensity can be measured with an optimum accuracy of 3%, whereas shifts in peak emission wavelength can be measured with an accuracy better than 0.1 nm (see legend to Fig. 2*b*). The accuracy of intensity measurements could be improved by enclosing the apparatus in a chamber so as to minimize turbulences around the sample. However, shifts in peak wavelength are expected to be of more interest, being more reproducible when the sample is changed since they are to a large extent insensitive to the amount of probed material.

Crystals that are optically too dense to record absorption spectra of any use are still amenable to fluorescence spectroscopy, as demonstrated in the case of PYP (Fig. 3). Emission spectra from the weakly fluorescent chromophore of PYP, although they mainly probe the crystal surface and may be distorted by inner filtering effects, are of outstanding signal to noise ratio, and reveal several features that could be useful for detailed studies on this system. Although a precise interpretation of these spectra is beyond the scope of this paper, they appear consistent with results obtained by Hoff *et al.* (1992), who described the low-temperature fluorescence of PYP in solution of 67% (vol./vol.) glycerol. Although influence of *e.g.* the glycerol content or the crystallization medium should be taken into account, fluorescence could be used to perform a comparative study of PYP in solution and in the crystalline form. Although PYP rapidly enters its photocycle upon blue light absorption, it seems likely that, at the used temperatures and under our conditions of illumination [compare with Genick *et al.* (1998) who used much longer light exposure], the spectra of Fig. 3 mostly originate from PYP in its ground-state conformation. However, the build-up of intermediate states along the PYP photocycle could potentially be followed by fluorescence under conditions of actinic illumination. Our results open the way to similar studies on crystals of other light-sensitive proteins. For example, bacteriorhodopsin was also demonstrated to be fluorescent at low temperature (Gillbro & Kriebel, 1979; Gillbro *et al.*, 1977; Gillbro & Sundström, 1983).

The temperature dependence of fluorescence emission appears of high interest. Firstly, the fluorescence quantum yield increases significantly when the temperature is lowered, because, as predicted by theory (Lakowicz, 1999), thermal relaxation pathways following photon absorption are less favoured. This observation could be a matter of concern when setting up protocols to populate intermediate states in crystals of light-sensitive proteins at cryo-temperatures. Indeed, fluorescence provides a bypass at these temperatures that may prevent an excited molecule to enter its photocycle. Although we did not attempt here to measure quantitatively the fluorescence quantum yield of PYP at 100 K, it appears unlikely from the literature (Hoff *et al.*, 1992) that it exceeds 0.1. This value is small but may not be negligible when compared to the photocycle quantum yield (0.65 at room temperature).

Secondly, a significant red shift of the emission maximum is observed as the temperature is raised. This shift results from an increase in the number of accessible vibration levels and/or from modifications in solvent relaxation effects (Lakowicz, 1999) as more thermal energy becomes available. Modification in fine structure (Fig. 3) might also result from changes in sample rigidity. Therefore, temperature-dependent fluorescence studies appear of high interest to probe dynamics in crystalline proteins. For example, we have obtained evidence that solvent transitions such as the glass transition (Vitkup *et al.*, 2000; Weik *et al.*, 2001) can be followed in this way (not shown). In particular as opposed to endogenous fluorophores located in the interior hydrophobic part of the protein, exogenous fluorophores can be used to probe the solvent channels and the two behaviours can be compared. These results will be published elsewhere.

As opposed to Fig. 3, Fig. 4 shows that molecules which are optically too transparent to be seen in an absorption spectrum may still be efficiently detected in protein crystals by fluorescence spectroscopy. The observation of the absorption spectrum recorded on the MalDH crystal could lead to the conclusion that no reduced NADH was present in the sample, likely due to a slow oxidation process. The strong absorption of aromatic amino acids at 280 nm prevented the observation of the strongest absorption line of NADH at *ca* 260 nm and a residual peak at 345 nm could not be detected with the available signal to noise ratio. On the contrary, a fluorescence spectrum left no doubt about the presence of residual NADH in the crystal. Based on the assumption that the fluorescence quantum yield of NADH in MalDH is similar to or greater than the one reported in solution (*ca* 0.02), we estimated that the optical density of NADH in this crystal amounted to no more than *ca* 0.025 OD. A larger quantum yield, as often observed for protein-bound NADH or due to the cryo-temperature, would imply an even lower OD. Such a small optical density could not be detected under the used conditions, since the r.m.s. noise level in the absorbance spectrum of Fig. 4 (about 0.02 OD) already reached this value. The fluorescence emission spectrum of this figure shows that the occupancy of NADH in the crystal, although small, was still significant, proving that oxidation of NADH in crystals of MalDH is a very slow process. Although it is not easy to assess the NADH occupancy in a quantitative way [polarized light should be used for this task (Hofrichter & Eaton, 1976)], the fact that the emission spectrum of Fig. 4 is largely above the detection limit demonstrates the considerable increase in sensitivity that can be achieved with fluorescence micro-spectrophotometry as compared to absorption micro-spectrophotometry.

Fig. 5 shows that fluorescence may also be used to measure the pH in samples as small as a protein crystal (*ca* 1 nl). It is known that the protonation state of fluorescein affects the absorption and fluorescence properties of this molecule, which can therefore be used as a pH indicator in solution (Yguerabide *et al.*, 1994). Since emission spectra from fluorescein are usually dominated by the di-anionic form of the molecule, the fluorescence intensity decreases as the pH is lowered. We also observed this behaviour in crystals of Tmpk (not shown). However, since in our case the fluorescence intensity is also dependent on sample volume and geometry, pH changes can only be measured reliably in this way if they are generated *in situ* within a unique sample. This would be the case if for example a pH jump was generated by liberating caged protons with UV light (Khan *et al.*, 1993), possibly at cryo-temperature (Ursby *et al.*, 2002). Proton release and diffusion throughout the sample could be monitored by recording the decay of fluorescence intensity.

Fig. 5 proves that at cryo-temperatures, it is possible to relate fluorescence and pH in a way that is essentially independent from emission intensity and peak wavelength, and which is based on evaluating the relative contributions to the spectra of the mono- and di-anionic form of fluorescein. Therefore the effect of pH can be mostly decoupled from the effects of other parameters such as sample volume or chemical environment. This technique only works at cryo-temperature, where the shoulder in emission spectra characteristic of the mono-anion contribution is clearly visible, probably due to the narrowed width of fluorescence lines when thermal energy is withdrawn. The fact that excited-state proton reactions are less likely to occur at such temperatures may also play a role (Yguerabide *et al.*, 1994). Fig. 5(*b*) shows that relative changes in pH (not absolute values at cryo-temperatures; see below) can be measured with a precision of at least 0.5 unit over the pH range 4.5–7.5, both in amorphous films of the Tmpk mother liquor and in crystals of the enzyme. The plot, which may be viewed as a crude titration curve, gives the impression that the pK between the mono- and di-anionic forms of fluorescein (pK_M = 6.3 at room temperature) decreases at 100 K to a value close to 5.5. This decrease is unlikely to be real, since pH values are reported as measured at room temperature and therefore are significantly underestimated at cryo-temperatures (the dissociation constant of the buffer is expected to decrease as the temperature is lowered). pH measurements could possibly be improved further by using pH indicators of higher performance, like Rhodol green or Oregon green.

Fluorescence from protein crystals may also find applications in the field of instrumentation. For example, fluorescence can greatly facilitate the localization of a crystal mounted in a large cryo-loop, and therefore its centring on an X-ray goniometer. We noticed that a low level of UV light at 355 nm was generally sufficient to excite residual fluorescence from aromatic amino acids, resulting in an enhanced contrast between the crystal and the mother liquor.

In conclusion, the described spectrophotometer allows one to collect fluorescence emission spectra from protein crystals with a high sensitivity. Although their information content generally differ, fluorescence spectra often surpass in quality the corresponding absorption spectra recorded on the same crystalline sample. Crystals that are optically too dense or too transparent to provide absorption spectra of any use may still be amenable to fluorescence spectroscopy. A further advantage of fluorescence when the bulk of an opaque sample has to be probed is that an excitation wavelength remote from the

absorption maximum may often be used. In the case of PYP, using an excitation wavelength at 355 nm instead of 455 nm allowed a gain by a factor of more than 350 in light transmission through the crystals. Although photo-bleaching resulted in this case, this is not expected to be the general rule. Photo-bleaching was not significantly increased when exciting at 355 nm with high concentrations of fluorescein. This corroborates calculations showing that the adiabatic temperature rise produced by a typical excitation pulse amounts to only a few tens of a Kelvin, assuming that the sample behaves like water and that all the absorbed energy dissipates as heat. Fluorescence from protein crystals opens the route to numerous experiments ranging from instrumentation to structural enzymology. An especially interesting application would be to attach fluorescence probes (*e.g.* thioreactive fluorophores), possibly using site-directed mutagenesis (*e.g.* with cysteines), at positions in the protein to be crystallized where fluorescence is modified along the reaction pathway (Boyd *et al.*, 2000). In this way, hints could be provided for trapping intermediate states in the crystal. Being sensitive to physico-chemical parameters such as temperature, viscosity or pH, the technique also appears of special interest for studies in protein dynamics.

Developments are in progress to enhance the performance of our spectrometer. Excitation of tryptophan fluorescence will soon be available. Polarized light will allow one to perform more quantitative measurements. Measuring fluorescence anisotropy will also help to discriminate the fluorescence signal originating from well ordered fluorophores (such as those bound to a macromolecule) from the signal originating from disordered fluorophores residing in the solvent. Likewise, more sophisticated fluorescence experiments could be envisaged, such as time-resolved fluorescence or experiments based on fluorescence resonance energy transfer.

The authors are grateful to M. Wulff and F. Schotte for early developments of the absorption spectrometer. We acknowledge R. Kort, J. Hendriks and K. J. Helliwerf for providing PYP crystals, and A. Irimia, M. Weik and G. Zaccai for providing MalDH crystals. We thank M. Weik for fruitful discussions and Philippe Charrault for technical assistance. This work was supported by the EU Biotechnology program BIO4-CT98-0354.

References

Boyd, A. E., Marnett, A. B., Wong, L. & Taylor, P. (2000). *J. Biol. Chem.* **275**, 22401–22408.
Chen, Y., Srajer, V., Ng, K., LeGrand, A. & Moffat, K. (1994). *Rev. Sci. Instrum.* **65**, 1506–1511.
Cohen, S. L. & Chait, B. T. (2001). *Annu. Rev. Biophys. Biomol. Struct.* **30**, 67–85.
Dahms, T. E. S. & Szabo, A. G. (1997). *Methods Enzymol.* **278**, 202–221.
Dahms, T. E. S., Willis, K. J. & Szabo, A. G. (1995). *J. Am. Chem. Soc.* **117**, 2321–2326.
Dym, O., Mevarech, M. & Sussman, J. L. (1995). *Science*, **267**, 1344–1346.
Eftink, M. R. (1997). *Methods Enzymol.* **278**, 221–257.
Eftink, M. R. & Shastry, M. C. (1997). *Methods Enzymol.* **278**, 258–286.
Garman, E. F. & Schneider, T. R. (1997). *J. Appl. Cryst.* **30**, 211–237.
Genick, U. K., Soltis, S. M., Kuhn, P., Canestrelli, I. L. & Getzoff, E. D. (1998). *Nature (London)*, **392**, 206–209.
Gillbro, T. & Kriebel, A. N. (1979). *FEBS Lett.* **79**, 29–32.
Gillbro, T., Kriebel, A. N. & Wild, U. P. (1977). *FEBS Lett.* **78**, 57–60.
Gillbro, T. & Sundström, V. (1983). *Photochem. Photobiol.* **37**, 445–455.
Hadfield, A. & Hajdu, J. (1993). *J. Appl. Cryst.* **26**, 839–842.
Hoff, W. D., Kwa, S. L. S., van Grondelle, R. & Hellingwerf, K. J. (1992). *Photochem. Photobiol.* **56**, 529–539.
Hofrichter, J. & Eaton, W. A. (1976). *Annu. Rev. Biophys. Bioeng.* **5**, 511–560.
Khan, S., Castellano, F., Spudich, J. L., McCray, J. A., Goody, R. S., Reid, G. P. & Trentham, D. R. (1993) *Biophys. J.* **65**, 2368–2382.
Karlsson, A., Parales. J. V., Parales, R. E, Gibson, D. T., Eklund, H. & Ramaswamy, S. J. (2000). *Inorg. Biochem.* **78**, 83–87.
Lakowicz, J. R. (1999). *Principles of Fluorescence Spectroscopy*, 2nd ed. New York: Kluwer/Plenum.
Langlois, R., Kim, S. H. & Cantor, C. R. (1975). *Biochemistry*, **14**, 2554–2558.
Mozzarelli, A. & Rossi G. L. (1996). *Annu. Rev. Biophys. Biomol. Struct.* **25**, 343–365.
Nicolet, Y., de Lacey, A. L., Vernede, X., Fernandez, V. M., Hatchikian, E. C. & Fontecilla-Camps, J. C. (2001). *J. Am. Chem. Soc.* **123**, 1596–1601.
Nurizzo, D., Cutruzzola, F., Arese, M., Bourgeois, D., Brunori, M., Cambillau C. & Tegoni, M. (1999). *J. Biol. Chem.* **274**, 14997–15004.
O'Hara, P., Goodwin, P. & Stoddard, B. L. (1995). *J. Appl. Cryst.* **28**, 829–834.
Perozzo, M. A., Ward, K. B., Thompson, R. B. & Ward, W. W. (1988). *J. Biol. Chem.* **263**, 7713–7716.
Petsko, G. A. & Ringe, D. (2000). *Curr. Opin. Chem. Biol.* **4**, 89–94.
Ren, Z., Perman, B., Srajer, V.,Teng, T.Y., Pradervand, C., Bourgeois, D., Schotte, F., Ursby, T., Wulff, M., Kort, R. & Moffat, K. (2001). *Biochemistry*, **40**, 13788–13801.
Royant, A., Edman, K., Ursby, T., Pebay-Peyroula, E., Landau, E. M. & Neutze, R. (2000). *Nature (London)*, **406**, 645–648.
Scheidig, A. J., Franken, S. M., Corrie, J. E. T., Reid, G. P., Wittinghofer, A., Pai, E. F. & Goody, R. S. (1995). *J. Mol. Biol.* **253**, 132–150.
Schlichting, I. (2000). *Acc. Chem. Res.* **33**, 532–538.
Schlichting, I., Rapp, G., John, J., Wittinghofer, A., Pai, E. F. & Goody, R. S. (1989). *Proc. Natl. Acad. Sci. USA*, **86**, 7687–7690.
Schotte, F. (2000). PhD thesis, pp. 54–55. Forschungzentrum Jülich GmbH.
Stoddard, B. L. & Farber, G. K. (1995). *Struct. Fold. Des.* **3**, 991–996.
Teng, T. Y. (1990). *J. Appl. Cryst.* **23**, 387–391.
Ursby, T., Weik, M., Fioravanti, E., Delarue, M., Goeldner, M. & Bourgeois, D. (2002). *Acta Cryst.* D**58**, 607–614.
Vitkup, D., Ringe, D., Petsko, G. A. & Karplus, M. (2000). *Nat. Struct. Biol.* **7**, 34–38.
Weik, M., Kryger, G., Schreurs, A. M. M., Bouma, B., Silman, I., Sussman, J. L., Gros, P. & Kroon, J. (2001). *Acta Cryst.* D**57**, 566–573.
Willis, K. J., Szabo, A. G. & Krajcarski, D. T. (1991). *J. Am. Chem. Soc.* **113**, 2000–2002.
Yguerabide, J., Talavera, E., Alvarez, J. M. & Quintero, B. (1994). *Photochem. Photobiol.* **60**, 435–441.